Fundamental PWM Excitation Based Rotor Position Estimation for a Dual Three-phase Permanent Magnet Synchronous Machine

Hao Chen, Qiang Gao*, *Member, IEEE, Tao Yang, Senior Member, IEEE* ,Mark Sumner, *Senior Member, IEEE*

***Abstract*—Two rotor position estimation methods for a dual three-phase (DTP) permanent magnet synchronous machine (PMSM) are investigated in this paper, where the rotor position is estimated by exploiting the saliency of the motor through the phase current derivative measurement during the fundamental PWM excitation of a standard six-phase two-level inverter. It is found that in a DTP PMSM, the wide speed range rotor position estimation is possible not only in the torque-producing sub-space, but also in the harmonic sub-space. The principle and practical implementation of the methods are explained in details. The experimental results verify the effectiveness of the proposed rotor position estimation methods.**

***Index Terms*—Dual three-phase PMSM, fundamental PWM excitation, sensorless control.**

I. Introduction

THE interest for multiphase AC machines has been growing in recent years. Compared with three-phase machines, multiphase machines have higher fault-tolerant capability, smaller torque ripple and lower requirement to the rating of individual power electronic devices, and therefore are more suitable for high power applications or safe-critical applications, such as off-shore wind power generation and electrified transportation, etc, [1]-[5]. A dual three-phase (DTP) permanent magnet synchronous machine (PMSM) is an attractive topology among different types of multiphase machines, partly because its inverter can be built directly from standard three-phase inverters.

A typical DTP PMSM has two sets of symmetrical stator windings, namely ABC and DEF, spatially shifted by 30 electrical degrees with two isolated neutral points. The DTP PMSM is supplied by a six-phase two-level inverter, as shown in Fig. 1.

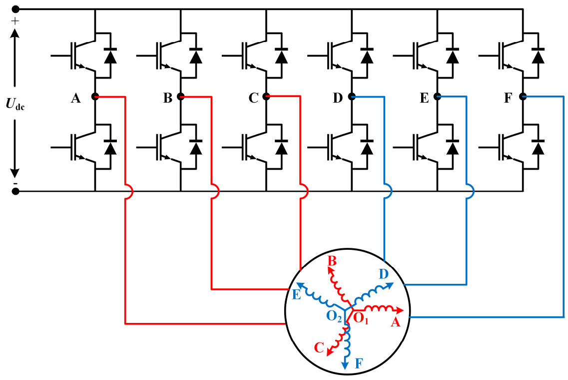

Fig. 1 Dual three-phase PMSM and six-phase two-level inverter

Similar to a three-phase AC machine, in order to obtain good closed-loop control performance of a DTP-PMSM, accurate rotor position or speed is required, which is generally obtained from mechanical sensors such as an encoder or a resolver mounted on the shaft. However, the mechanical sensors will increase the cost and volume of the drive system, and reduce the reliability. In some cases, mechanical sensors are not suitable to be installed. Therefore, sensorless control of a DTP-PMSM has been paid much attention in recent years.

A variety of methods to estimate the rotor position/speed of a DTP-PMSM have been reported, and they can be broadly divided into two categories.

The first category makes use of the fundamental model of the DTP-PMSM to estimate the rotor position or speed, e.g. [6-13].

Some researchers estimated the rotor position by measuring/observing the back EMF of the machine. For

This paragraph of the first footnote will contain the date on which you submitted your paper for review, which is populated by IEEE. This work was supported in part by the National Nature Science Foundation of China (NSFC) under Grant 51477101. *Corresponding author: Qiang Gao.*

Hao Chen and Qiang Gao are both with the Department of Electrical Engineering, School of Electronic Information and Electrical Engineering, Shanghai Jiao Tong University, Shanghai 200240, China, and also with the Key Laboratory of Control of Power Transmission and Conversion, Ministry of Education, Shanghai Jiao Tong University, Shanghai 200240, China (e-mails: hchen0@sjtu.edu.cn, gaoqiang@sjtu.edu.cn).

Tao Yang and Mark Sumner are both with the University of Nottingham, University Park, Nottingham, NG7 2RD, U.K (e-mails: tao.yang@nottingham.ac.uk, mark.sumner@nottingham.ac.uk).

Color versions of one or more of the figures in this article are available online at http://ieeexplore.ieee.org

instance, in [6], the currents of one set of three-phase windings were set to zero for a short time to measure back EMF directly to reduce the influence of magnetic saturation and temperature on the flux observer. Simulation was conducted at 7.96 Hz with a load of 8 Nm, and the estimation error was less than 0.1 rad. In [7-8], two methods based on third harmonic back EMF were used, i.e. the method using flux combined with Extended Kalman Filter and the method using third harmonic back EMF directly to estimate rotor position. Experiments were conducted at 16.67 Hz with a 1 A q-axis current, and the estimation errors were both less than 0.1 rad.

Meanwhile, the model reference adaptive system (MRAS) method was adopted by some researchers. In [9], the MRAS method was adopted and an experiment was conducted with a 25% rated load and the speed was varied from 50% to 70% rated speed to verify the effectiveness of the method. In [10], the MRAS method was used in an aircraft electric starter/generator system. Simulation was conducted at the speed of 900 Hz and the estimation error was less than 3.5×10^{-5} rad.

Some researchers resorted to different observers or the Kalman filter (EKF). For example, in [11], two methods, i.e. PLL observer and Luenberger observer were compared. Simulations were conducted at 900 Hz with the load ranging from 0 Nm to 14.8 Nm. The estimation errors were both less than 0.2 rad. The simulation results showed that Luenberger observer had better dynamic performance but was vulnerable to high frequency noise, while the PLL observer was insensitive to high frequency noise due to its low-pass characteristics. In [12], a flux observer (FO) and an extended Kalman filter (EKF) were compared. Experiments were conducted at 25 Hz with a 1.8 Nm load, and the estimation errors were both less than 0.05rad. Experimental results showed that EKF method was less sensitive to harmonics in the back EMF, and had lower torque ripple and current harmonic than the FO. In [13], the sliding mode observer (SMO) was used to estimate the back EMF, and the traditional low pass filter was replaced by synchronous frequency tracking filter to obtain the fundamental component in the back EMF. Simulation was conducted at 1800 Hz with a 40 Nm load, and the estimation error was less than 0.1rad.

While these methods are all suitable for medium or high speed applications, their performance tends to deteriorate at low and zero speeds due to the poor signal to noise ratio (SNR), which is similar to those methods for a three-phase PMSM, e.g. [14]. Besides, the accuracy of these methods relies on the accurate machine parameters, which usually vary seriously during operation, and on-line compensation for parameters changes is also required, which increases the complexity of these methods.

In order to achieve the low and zero speed operation, the second category of methods, i.e., the high frequency injection based methods have been proposed [15-22]. These methods rely on the saliency of the machine.

In [15], the rotor position estimation for a symmetrical DTP-PMSM was investigated using the high frequency voltage injection, which is slighted adapted from the classical scheme for a three-phase machine. Position estimation under torque-controlled operation were conducted from 0-95.5 Hz, and the estimation error was less than 0.35 rad. It is not clear whether the results were obtained in sensorless mode, and no closed-loop speed sensorless operation was presented. In [16] and [17], the high frequency voltage injection method was applied on a DTP fraction-slot PMSM. Experiments were conducted at 8.33 Hz with loads at 3.8 Nm and 1.9Nm, while the estimation errors were both less than 0.25 rad. In [16], high frequency voltage injection based on Extended Electromotive Force Model was investigated for a DTP-PMSM. Simulation was conducted at 2.67 Hz with a rated load, and the estimation error was less than 0.1rad. In [19], high frequency voltage signal was only injected to one set of three-phase windings, and experiment was conducted at 5 Hz to verify the effectiveness. In [20], rotating carrier signal injection utilizing zero-sequence carrier voltage method was used, and the phase shift between the two voltage signals injected to the two sets of windings was adjusted to reduce estimation error caused by harmonics in zero-sequence voltage. Experiments were conducted at 2.5 Hz, and the estimation error was less than 0.2 rad. In [21], the pulsating signal injection using zero-sequence carrier voltage method was investigated. Experiments were conducted at 2.5 Hz, and the estimation error was less than 0.1 rad. In [22], a position error correction method based on current pulse injection was investigated. Experiments were conducted at 8 Hz and the estimation error was less than 0.1 rad.

Methods of rotor position estimation of a three-phase motor using the transient excitation of the fundamental PWM waveforms of an inverter were illustrated in [23-25, etc], and their applicability to a DTP-PMSM has been initially studied in [26-27], where its principle along with simulation results and preliminary experimental results at low and zero speeds were demonstrated. In this paper, the results of further research on this topic are presented. First of all, position estimation at not only low and zero speeds, but also at higher speed, in the *α-β* subspace is studied experimentally. Furthermore, the unique feature for a multiphase motor, i.e., the potential of position estimation of a DTP-PMSM in the *x-y* subspace within a wide speed range is also exploited.

The contribution of this work is listed below:

- Instead of deriving a rotor position estimation algorithm in the nature stationary frame, which was implemented in [21] for a three-phase AC machine, this work presents a more general approach in the two-phase stationary frame. This general approach greatly eases the efforts of derivation and implementation, when the phase number increases.
- it is found out that in its harmonic sub-space of a multi-phase machine, the implementation of rotor position estimation becomes easier, since measuring the di/dt of a zero vector becomes unnecessary, even at higher speeds.

The rest of the paragraphs are organized as follows. In Section II, principles of the position estimation in the *α-β* and *x-y* subspaces are introduced. In Section III, key implementation issues to achieve good position estimation are presented. In Section IV, experimental results within a wide speed range are illustrated. In Section V, the rotor position estimation methods in the two sub-spaces and their results are discussed and summarized.

II. POSITION ESTIMATION PRINCIPLES

A. Principle of the Vector Space Decomposition (VSD) Method

The Vector Space Decomposition method was first proposed in [28]. A conversion matrix T_s is used to map the six-phase stationary coordinate system into three two-dimensional subspaces, namely α-β subspace, x-y subspace (i.e., z1-z2 subspace in [28]) and o1-o2 subspace. All electromechanical energy conversion related variables are mapped into the *α-β* subspace, and the non-electromechanical energy conversion related variables are transformed to the x-y subspace and the *o1-o2* subspace. The constant power conversion matrix T_s used in this paper is shown as (1):

$$\boldsymbol{T}_s = \frac{1}{\sqrt{3}}\begin{bmatrix} 1 & -\frac{1}{2} & -\frac{1}{2} & \frac{\sqrt{3}}{2} & -\frac{\sqrt{3}}{2} & 0 \\ 0 & \frac{\sqrt{3}}{2} & -\frac{\sqrt{3}}{2} & \frac{1}{2} & \frac{1}{2} & -1 \\ 1 & -\frac{1}{2} & -\frac{1}{2} & -\frac{\sqrt{3}}{2} & \frac{\sqrt{3}}{2} & 0 \\ 0 & -\frac{\sqrt{3}}{2} & \frac{\sqrt{3}}{2} & \frac{1}{2} & \frac{1}{2} & -1 \\ 1 & 1 & 1 & 0 & 0 & 0 \\ 0 & 0 & 0 & 1 & 1 & 1 \end{bmatrix} \quad (1)$$

The T_s matrix is used for mapping from six-phase stationary coordinate to the *αβ-xy-o1o2* reference frame. The transformation is shown as (2):

$$[f_\alpha \ f_\beta \ f_x \ f_y f_{o1} \ f_{o2}]^{\mathrm{T}} = T_s[f_A \ f_B \ f_C \ f_D f_E \ f_F]^{\mathrm{T}} \quad (2)$$

Here, f_α refers to voltage or current projected in the α axis and so on. f_A refers to voltage and current projected in the A axis and so on.

Then the mathematic model of DTP PMSM in six-phase PMSM can be converted into the *α-β* subspace and the *x-y* subspace. Since the two neutral points are isolated for a typical DTP PMSM, components in the *o1-o2* subspace are zero [28].

B. Principle of the Rotor Position Estimation Method in the α-β Subspace

Using the VSD method, the original mathematical model of a DTP PMSM in the natural six-phase coordinate can be mapped into *α-β* subspace, which is written as (3):

$$\begin{aligned}\begin{bmatrix} u_\alpha \\ u_\beta \end{bmatrix} &= R\begin{bmatrix} i_\alpha \\ i_\beta \end{bmatrix} + \\ &\omega_e\begin{bmatrix} -2L_{\alpha\beta2}\sin 2\theta & 2L_{\alpha\beta2}\cos 2\theta \\ 2L_{\alpha\beta2}\cos 2\theta & 2L_{\alpha\beta2}\sin 2\theta \end{bmatrix}\begin{bmatrix} i_\alpha \\ i_\beta \end{bmatrix} + \\ &\begin{bmatrix} L_{\alpha\beta1} + L_{\alpha\beta2}\cos 2\theta & L_{\alpha\beta2}\sin 2\theta \\ L_{\alpha\beta2}\sin 2\theta & L_{\alpha\beta1} - L_{\alpha\beta2}\cos 2\theta \end{bmatrix}\begin{bmatrix} \frac{\mathrm{d}i_\alpha}{\mathrm{d}t} \\ \frac{\mathrm{d}i_\beta}{\mathrm{d}t} \end{bmatrix} + \\ &\begin{bmatrix} \psi_f\omega_e\cos\theta \\ \psi_f\omega_e\sin\theta \end{bmatrix}\end{aligned} \quad (3)$$

where u_α, u_β and i_α, i_β are projections of phase voltage and current vectors along the α-axis and β-axis; $L_{\alpha\beta1}$, $L_{\alpha\beta2}$ are inductances in the *α-β* subspace, depicting the average and amplitude of the variable part of the inductances; R is the winding resistor per phase; ψ_f is the PM flux linkage per phase; ω_e is the electrical speed, and θ is the electrical rotor position. From Equ (3), one may find that the rotor position signals (*sin2θ* and *cos2θ*) are coupled with rotor speed, and it indicates that rotor position estimation is possible only at low and zero speeds if only active vectors are considered.

Eq. (3) is valid for all the voltage space vectors of a six-phase two-level inverter. When a zero voltage vector is applied, the voltage equation is expressed as (4):

$$\begin{aligned}\begin{bmatrix} 0 \\ 0 \end{bmatrix} &= R\begin{bmatrix} i_{\alpha0} \\ i_{\beta0} \end{bmatrix} + \\ &\omega_e\begin{bmatrix} -2L_{\alpha\beta2}\sin 2\theta & 2L_{\alpha\beta2}\cos 2\theta \\ 2L_{\alpha\beta2}\cos 2\theta & 2L_{\alpha\beta2}\sin 2\theta \end{bmatrix}\begin{bmatrix} i_{\alpha0} \\ i_{\beta0} \end{bmatrix} + \\ &\begin{bmatrix} L_{\alpha\beta1} + L_{\alpha\beta2}\cos 2\theta & L_{\alpha\beta2}\sin 2\theta \\ L_{\alpha\beta2}\sin 2\theta & L_{\alpha\beta1} - L_{\alpha\beta2}\cos 2\theta \end{bmatrix}\begin{bmatrix} \frac{\mathrm{d}i_{\alpha0}}{\mathrm{d}t} \\ \frac{\mathrm{d}i_{\beta0}}{\mathrm{d}t} \end{bmatrix} + \\ &\begin{bmatrix} \psi_f\omega_e\cos\theta \\ \psi_f\omega_e\sin\theta \end{bmatrix}\end{aligned} \quad (4)$$

Assuming variation of the rotor position and the current is neglectable during one PWM period, i.e., $i_\alpha \approx i_{\alpha0}$, $i_\beta \approx i_{\beta0}$, then (5) can be obtained by subtracting (4) from (3):

$$\begin{aligned}\begin{bmatrix} u_\alpha \\ u_\beta \end{bmatrix} &= \begin{bmatrix} L_{\alpha\beta1} + L_{\alpha\beta2}\cos 2\theta & L_{\alpha\beta2}\sin 2\theta \\ L_{\alpha\beta2}\sin 2\theta & L_{\alpha\beta1} - L_{\alpha\beta2}\cos 2\theta \end{bmatrix} \times \\ &\begin{bmatrix} \frac{\mathrm{d}i_\alpha}{\mathrm{d}t} - \frac{\mathrm{d}i_{\alpha0}}{\mathrm{d}t} \\ \frac{\mathrm{d}i_\beta}{\mathrm{d}t} - \frac{\mathrm{d}i_{\beta0}}{\mathrm{d}t} \end{bmatrix}\end{aligned} \quad (5)$$

From (5), (6) can be derived.

$$\begin{aligned}&\frac{L_{\alpha\beta1}^2 - L_{\alpha\beta2}^2}{L_{\alpha\beta2}}\left(u_\beta\left(\frac{\mathrm{d}i_\alpha}{\mathrm{d}t} - \frac{\mathrm{d}i_{\alpha0}}{\mathrm{d}t}\right) - u_\alpha\left(\frac{\mathrm{d}i_\beta}{\mathrm{d}t} - \frac{\mathrm{d}i_{\beta0}}{\mathrm{d}t}\right)\right) \\ &= (u_\alpha^2 - u_\beta^2)\sin 2\theta - 2u_\alpha u_\beta\cos 2\theta\end{aligned} \quad (6)$$

According to the conventional four-space-vector pulse width modulation (SVPWM) scheme in [28], there are four different active voltage vectors in a PWM period, which are selected from the twelve voltage vectors with the maximum amplitude. Considering any two active voltage vectors within a PWM cycle, e.g. the first and the second in a PWM sequence, equation (7) can be obtained from (6):

$$\begin{aligned}&\frac{L_{\alpha\beta1}^2 - L_{\alpha\beta2}^2}{L_{\alpha\beta2}}\begin{bmatrix} u_{\beta1}\left(\frac{\mathrm{d}i_{\alpha1}}{\mathrm{d}t} - \frac{\mathrm{d}i_{\alpha0}}{\mathrm{d}t}\right) - u_{\alpha1}\left(\frac{\mathrm{d}i_{\beta1}}{\mathrm{d}t} - \frac{\mathrm{d}i_{\beta0}}{\mathrm{d}t}\right) \\ u_{\beta2}\left(\frac{\mathrm{d}i_{\alpha2}}{\mathrm{d}t} - \frac{\mathrm{d}i_{\alpha0}}{\mathrm{d}t}\right) - u_{\alpha2}\left(\frac{\mathrm{d}i_{\beta2}}{\mathrm{d}t} - \frac{\mathrm{d}i_{\beta0}}{\mathrm{d}t}\right) \end{bmatrix} \\ &= \begin{bmatrix} -2u_{\alpha1}u_{\beta1} & u_{\alpha1}^2 - u_{\beta1}^2 \\ -2u_{\alpha2}u_{\beta2} & u_{\alpha2}^2 - u_{\beta2}^2 \end{bmatrix}\begin{bmatrix} \cos 2\theta \\ \sin 2\theta \end{bmatrix}\end{aligned} \quad (7)$$

where $u_{\alpha1}$, $u_{\beta1}$, $i_{\alpha1}$, $i_{\beta1}$ and $u_{\alpha2}$, $u_{\beta2}$, $i_{\alpha2}$, $i_{\beta2}$ are voltages and currents during the first and the second active voltage vectors.

Due to the saliency effect of the machine, either from the saturation or from the rotor structural, which is the case in this work, a DTP PMSM has a $L_d < L_q$, which are related with $L_{\alpha\beta2}$ by (8):

$$L_{\alpha\beta2} = (L_d - L_q)/2 \tag{8}$$

Thus, $L_{\alpha\beta2} \neq 0$. Then the solution of (7) is obtained as in (9):

$$\begin{cases} c_1 sin2\theta = \dfrac{\left\{\begin{aligned} & u_{\alpha2}u_{\beta2}\left[u_{\beta1}\left(\frac{di_{\alpha1}}{dt}-\frac{di_{\alpha0}}{dt}\right)-u_{\alpha1}\left(\frac{di_{\beta1}}{dt}-\frac{di_{\beta0}}{dt}\right)\right] \\ & -u_{\alpha1}u_{\beta1}\left[u_{\beta2}\left(\frac{di_{\alpha2}}{dt}-\frac{di_{\alpha0}}{dt}\right)-u_{\alpha2}\left(\frac{di_{\beta2}}{dt}-\frac{di_{\beta0}}{dt}\right)\right]\end{aligned}\right\}}{\left[u_{\alpha1}u_{\beta1}\left(u_{\beta2}^2-u_{\alpha2}^2\right)-u_{\alpha2}u_{\beta2}\left(u_{\beta1}^2-u_{\alpha1}^2\right)\right]} \\ c_1 cos2\theta = \dfrac{\left\{\begin{aligned} & \left(u_{\alpha2}^2-u_{\beta2}^2\right)\left[u_{\beta1}\left(\frac{di_{\alpha1}}{dt}-\frac{di_{\alpha0}}{dt}\right)-u_{\alpha1}\left(\frac{di_{\beta1}}{dt}-\frac{di_{\beta0}}{dt}\right)\right] \\ & -\left(u_{\alpha1}^2-u_{\beta1}^2\right)\left[u_{\beta2}\left(\frac{di_{\alpha2}}{dt}-\frac{di_{\alpha0}}{dt}\right)-u_{\alpha2}\left(\frac{di_{\beta2}}{dt}-\frac{di_{\beta0}}{dt}\right)\right]\end{aligned}\right\}}{2\left[u_{\alpha1}u_{\beta1}\left(u_{\beta2}^2-u_{\alpha2}^2\right)-u_{\alpha2}u_{\beta2}\left(u_{\beta1}^2-u_{\alpha1}^2\right)\right]} \end{cases}$$

(9)

where $c_1 = {}^{L_{\alpha\beta2}}\big/\left(L_{\alpha\beta1}^2 - L_{\alpha\beta2}^2\right)$

From (9), one can see that if the voltage vectors are known, which is the case for the SVPWM modulation of a DTP PMSM drive, and the current derivatives can be measured, the position signals $c_1 sin2\theta$ and $c_1 cos2\theta$ can be obtained. Similar conclusion can be drawn from (12) in the next Subsection.

.

C. Principle of the Rotor Position Estimation Method in the x-y Subspace

The magnetic saturation modulates the total inductance of a DTP-PMSM, it is therefore assumed that the leakage inductances vary similarly with the inductance

The mathematical model of a DTP PMSM in the x-y subspace can be written as (10):

$$\begin{bmatrix} u_x \\ u_y \end{bmatrix} = R\begin{bmatrix} i_x \\ i_y \end{bmatrix} + \omega_e \begin{bmatrix} -2L_{xy2}\sin 2\theta & 2L_{xy2}\cos 2\theta \\ 2L_{xy2}\cos 2\theta & 2L_{xy2}\sin 2\theta \end{bmatrix}\begin{bmatrix} i_x \\ i_y \end{bmatrix} + \begin{bmatrix} L_{xy1} - L_{xy2}\cos 2\theta & L_{xy2}\sin 2\theta \\ L_{xy2}\sin 2\theta & L_{xy1} + L_{xy2}\cos 2\theta \end{bmatrix}\begin{bmatrix} \frac{di_x}{dt} \\ \frac{di_y}{dt} \end{bmatrix} \tag{10}$$

where u_x, u_y and i_x, i_y are projections of phase voltage and current vectors along the x-axis and y-axis; L_{xy1} and L_{xy2} are inductance in the x-y subspace, depicting the average and amplitude of the variable part of the inductances.

In order to reduce losses in a DTP PMSM, currents in the x-y subspace should be controlled to zero by proper current control loops, meaning $i_x \approx 0$ and $i_y \approx 0$. Then (10) can be simplified to (11):

$$\begin{bmatrix} u_x \\ u_y \end{bmatrix} = \begin{bmatrix} L_{xy1} - L_{xy2}\cos 2\theta & L_{xy2}\sin 2\theta \\ L_{xy2}\sin 2\theta & L_{xy1} + L_{xy2}\cos 2\theta \end{bmatrix}\begin{bmatrix} \frac{di_x}{dt} \\ \frac{di_y}{dt} \end{bmatrix} \tag{11}$$

Equation (11) is similar with (5), thus similar solutions can be obtained, as in (12):

$$\begin{cases} C_2 sin2\theta = \dfrac{-u_{x2}u_{y2}\left(u_{y1}\frac{di_{x1}}{dt} - u_{x1}\frac{di_{y1}}{dt}\right) + u_{x1}u_{y1}\left(u_{y2}\frac{di_{x2}}{dt} - u_{x2}\frac{di_{y2}}{dt}\right)}{u_{x1}u_{y1}\left(u_{x2}^2 - u_{y2}^2\right) - u_{x2}u_{y2}\left(u_{x1}^2 - u_{y1}^2\right)} \\ C_2 cos2\theta = \dfrac{\left(u_{x2}^2 - u_{y2}^2\right)\left(u_{y1}\frac{di_{x1}}{dt} - u_{x1}\frac{di_{y1}}{dt}\right) - \left(u_{x1}^2 - u_{y1}^2\right)\begin{pmatrix} u_{y2}\frac{di_{x2}}{dt} - \\ u_{x2}\frac{di_{y2}}{dt} \end{pmatrix}}{2u_{x1}u_{y1}\left(u_{x2}^2 - u_{y2}^2\right) - 2u_{x2}u_{y2}\left(u_{x1}^2 - u_{y1}^2\right)} \end{cases}$$

(12)

Where $c_2 = {}^{L_{xy2}}\big/\left(L_{xy1}^2 - L_{xy2}^2\right)$

It seems nature to use the arctan function to solve $\hat{\theta}$ directly from (9) or (12), as shown in (13):

$$\hat{\theta} = \frac{1}{2}arctan2\left(\frac{sin2\theta}{cos2\theta}\right) \tag{13}$$

However, there may exist high-frequency noise in the calculated $sin2\theta$ and $cos2\theta$ due to the sampling noise when calculating di/dt, which makes the implementation of (13) not practical. In this paper, a simple phase lock loop (PLL) is used to obtain $\hat{\theta}$ for the demonstration purpose. The PLL block diagram is shown in Fig. 2.

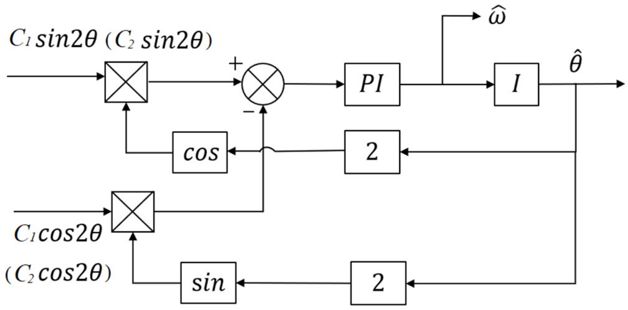

Fig. 2 PLL block diagram

From (11), one may notice that there are no items coupled with the speed, which means the rotor position estimation in the x-y subspace is hardly affected by the speed, and therefore the rotor position estimation is valid from low to high speeds. This feature is favourable because for the rotor position estimation at very high speed using the method in the α-β subspace, the duration of zero vector might not be long enough for current sampling. It should be emphasized that, in order to minimize the position estimation error, a proper current controller in the x-y subspace should designed. This could be either a classical PI controller or other more complicated schemes, such as [29].

III. KEY IMPLEMENTATION ISSUES

From (9) and (12), it can be seen that it is essential to obtain the current derivatives (di/dts) for the position signals' construction. In order to avoid installation of any di/dt sensors, a current difference (Δi) of a fixed time interval (Δt) is used to approximate the current derivative, i.e., di/dt≈Δi/Δt. Thus, accurate current measurement becomes paramount. However, the sample currents are easily prone to the switching noise of the inverter and the sampling noise at the ADC stage. In order to minimize these negative factors, several measures are taken:

- a minimum pulse width of the active vectors is enforced to avoid the switching noise;
- the least square method is adopted to filter the sampling noise.

In accompany with the first measure, a proper delay between the current sampling instants and the switching instants is also suggested.

More details of the above measures are described in the follows.

A. Minimum Pulse Width and Its Compensation Method

In this paper, the current derivatives corresponding to the first two active voltage vectors within a PWM cycle are measured. However, at low speeds or during the sector transition of the voltage space vector, the duration of the two voltage vectors may be too short to achieve accurate Δi measurement due to the limited ADC precision. Besides, upon turn-on/off of power transistors, current oscillations will appear due to the parasitic capacitance and inductance. To avoid these oscillations, the sampling point should be delayed. Because of the above two reasons, the dwell time of first two active voltage vectors should have a lower limit, termed minimum pulse width t_{min}. When the dwell time of either of the two voltage vectors is shorter than t_{min}, it will be extended to t_{min}.

However, this will lead to a deviation in the reference voltage vector, which will deteriorate the current control. In order to maintain the reference voltage vector, a simple compensation method is proposed in this work.

In this paper, the compensation principle is to extend the dwell time of each phase's PWM waveform according to the sector where the reference voltage vector is located, and the aim is to make the dwell time (excluding the zero voltage vectors' dwell times) of each phase's PWM waveform extended by the same value, text, while the dwell times of the first two active vectors will be kept no less than t_{min}. The definition of text is given by (14):

$$t_{\text{ext}} = \max(0, t_{\min} - t_1) + \max(0, t_{\min} - t_2) \quad (14)$$

The compensation method when the reference voltage vector is located in Sector 1 is shown in Fig.3. In Fig.3, the red and blue correspond to PWM waveforms before and after compensation respectively, when the case that t_1 and t_2 are both less than t_{min} is considered. The light-colored block's width is t_{min} - t_1, while the deep-colored block's width is t_{min} - t_2. The dwell times of the PWM waveforms (excluding zero voltage vectors' dwell time) in Fig.3 are shown in Table I.

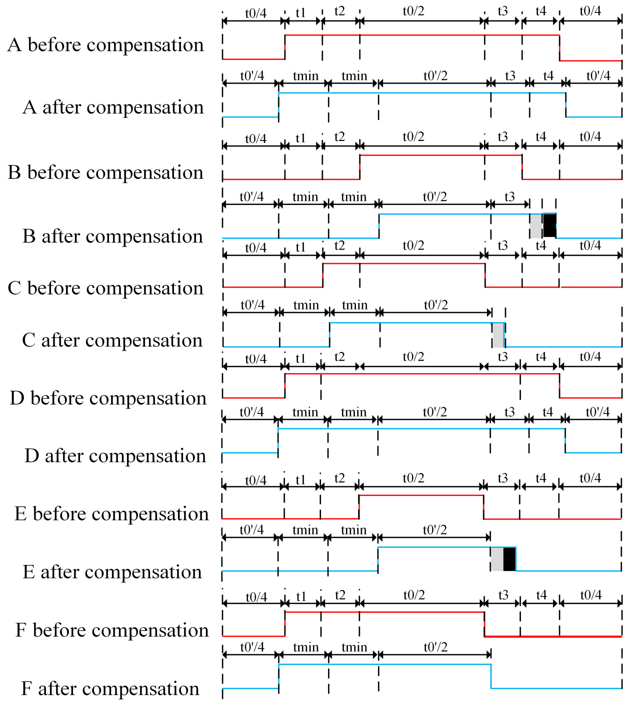

Fig. 3 PWM waveforms before and after compensation when the reference voltage vector lies in Sector 1

TABLE I
Dwell times of each phase's PWM waveform in Fig.3 (excluding the zero voltage vectors' dwell times)

Phase	Before compensation	After compensation
A	$t_1+t_2+t_3+t_4$	$2t_{min}+t_3+t_4$
B	t_3	$t_3+2t_{min}-t_1-t_2$
C	t_2	$2t_{min}-t_1$
D	$t_1+t_2+t_3+t_4$	$2t_{min}+t_3+t_4$
E	0	$2t_{min}-t_1-t_2$
F	t_1+t_2	$2t_{min}$

The compensation process contains two steps:

(1) t_1 and t_2 are extended to t_{min}.

(2) Check each phase's PWM waveform and make the dwell time (excluding zero vector) extended by text compared with the waveform before compensation.

Take phase A as an example. Suppose the initial dwell times of the first two active vectors before compensation are t_1 and t_2 respectively, and both are shorter than t_{min}. According to step (1), they are both extended to t_{min}. For phase B, the dwell time (excluding zero vector) before compensation is t_3, thus it needs to be extended to text, indicated by the sum of the light-colored and deep-colored blocks in Fig.3.

The correctness of this compensation method can be proved by volt-second product balance principle as follows.

The composite voltage vector in the α-β subspace and in the x-y subspace can be written as (15) and (16) [30]:

$$v_{\alpha\beta} = \frac{1}{3}U_{\mathrm{dc}}(s_{\mathrm{A}} + s_{\mathrm{B}}e^{\mathrm{j}\frac{2}{3}\pi} + s_{\mathrm{C}}e^{\mathrm{j}\frac{4}{3}\pi} + s_{\mathrm{D}}e^{\mathrm{j}\frac{\pi}{6}} + s_{\mathrm{E}}e^{\mathrm{j}\frac{5}{6}\pi} + s_{\mathrm{F}}e^{\mathrm{j}\frac{3}{2}\pi})$$

(15)

$$v_{\mathrm{xy}} = \frac{1}{3}U_{\mathrm{dc}}(s_{\mathrm{A}} + s_{\mathrm{B}}e^{\mathrm{j}\frac{4}{3}\pi} + s_{\mathrm{C}}e^{\mathrm{j}\frac{2}{3}\pi} + s_{\mathrm{D}}e^{\mathrm{j}\frac{5\pi}{6}} + s_{\mathrm{E}}e^{\mathrm{j}\frac{\pi}{6}} + s_{\mathrm{F}}e^{\mathrm{j}\frac{3}{2}\pi})$$

(16)

where U_{dc} is the voltage of DC bus of the inverter. s_i (i=A, B, C, D, E, F) refers to the state of the upper power transistor, with s_i=1 meaning that the upper power transistor is ON while the lower power transistor is OFF, and vice versa for s_i =0.

Thus, the volt-second products of the composite voltage vector in *α-β* subspace and *x-y* subspace are as (17) and (18):

$$v_{\alpha\beta} \times t_{\mathrm{PWM}} = \frac{1}{3}U_{\mathrm{dc}}(t_{\mathrm{A}} + t_{\mathrm{B}}e^{\mathrm{j}\frac{2}{3}\pi} + t_{\mathrm{C}}e^{\mathrm{j}\frac{4}{3}\pi} + t_{\mathrm{D}}e^{\mathrm{j}\frac{\pi}{6}} + t_{\mathrm{E}}e^{\mathrm{j}\frac{5\pi}{6}} + t_{\mathrm{F}}e^{\mathrm{j}\frac{3\pi}{2}}) \quad (17)$$

$$v_{\mathrm{xy}} \times t_{\mathrm{PWM}} = \frac{1}{3}U_{\mathrm{dc}}(t_{\mathrm{A}} + t_{\mathrm{B}}e^{\mathrm{j}\frac{4}{3}\pi} + t_{\mathrm{C}}e^{\mathrm{j}\frac{2}{3}\pi} + t_{\mathrm{D}}e^{\mathrm{j}\frac{5\pi}{6}} + t_{\mathrm{E}}e^{\mathrm{j}\frac{\pi}{6}} + t_{\mathrm{F}}e^{\mathrm{j}\frac{3\pi}{2}}) \quad (18)$$

where t_i (i=A, B, C, D, E, F) is the conduction time of phase i.

As mentioned before, after compensation the dwell time (excluding zero voltage vector) of each phase will be extended by the same value text, and thus the change in the volt-second product in the *α-β* subspace and the *x-y* subspace are given as in (19) and (20):

$$\frac{1}{3}U_{\mathrm{dc}}(t_{\mathrm{ext}} + t_{\mathrm{ext}}e^{\mathrm{j}\frac{2}{3}\pi} + t_{\mathrm{ext}}e^{\mathrm{j}\frac{4}{3}\pi} + t_{\mathrm{ext}}e^{\mathrm{j}\frac{\pi}{6}} + t_{\mathrm{ext}}e^{\mathrm{j}\frac{5\pi}{6}} + t_{\mathrm{ext}}e^{\mathrm{j}\frac{3\pi}{2}}) = 0 \quad (19)$$

$$\frac{1}{3}U_{\mathrm{dc}}(t_{\mathrm{ext}} + t_{\mathrm{ext}}e^{\mathrm{j}\frac{4}{3}\pi} + t_{\mathrm{ext}}e^{\mathrm{j}\frac{2}{3}\pi} + t_{\mathrm{ext}}e^{\mathrm{j}\frac{5\pi}{6}} + t_{\mathrm{ext}}e^{\mathrm{j}\frac{\pi}{6}} + t_{\mathrm{ext}}e^{\mathrm{j}\frac{3\pi}{2}}) = 0 \quad (20)$$

Since zero voltage vectors also do not have effect on the volt-second, the change of zero voltage vectors dwell times can be ignored.

It can be concluded therefore that the compensation method will not change the volt-second product. The procedure of this compensation method is shown in Fig.4 with both t_1 and t_2 less than t_{min}.

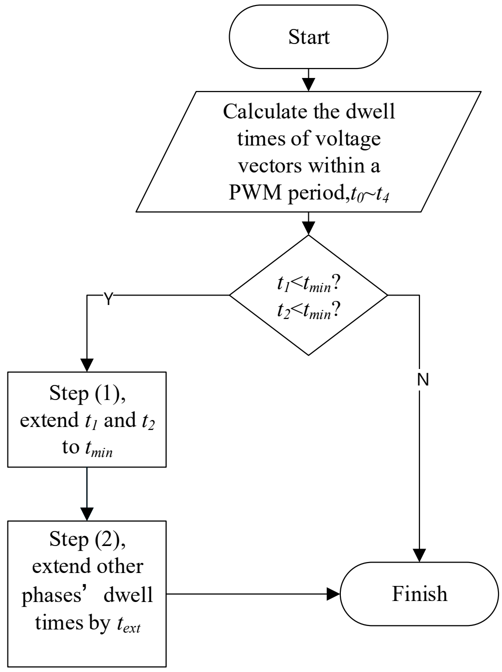

Fig.4 Flowchart of voltage vector extension and compensation method

B. *Oversampling with the Least Square Method*

The two-point method is an easy way to measure the current difference. However, it could be prone to the noise during the measurement. Therefore, the oversampling technique with the least square method [31-32] is adopted in this paper.

The phase current within part of a PWM period is shown in Fig. 5 correspond to a 20 us minimum pulse width. In Fig.5, PWM1 and PWM2 were only used to trigger ADC sampling.

During one voltage vector, *n* samples will be obtained successively with an equal interval. According to the least square linear model, *Δi* can be calculated as (21).

$$\Delta i = \Delta t \sum_{k=0}^{n-1}(t_{\mathrm{k}} - \bar{t})(i_{\mathrm{k}} - \bar{i}) / \sum_{k=0}^{n-1}(t_{\mathrm{k}} - \bar{t})^2 \quad (21)$$

where $t_{\mathrm{k}} = t_0 + k\Delta t / n$, $\bar{t} = \sum_{k=0}^{n-1} t_{\mathrm{k}} / n$, $\bar{i} = \sum_{k=0}^{n-1} i_{\mathrm{k}} / n$.

Equation (21) can be simplified and *t* can be eliminated as (22):

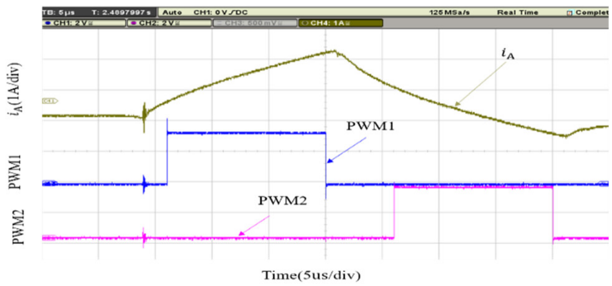

Fig.5 Current waveform within part of a PWM period

$$\Delta i = 12\sum_{k=0}^{n-1}(k - \frac{n-1}{2})(i_{\mathrm{k}} - \bar{i}) / (n(n+1)) \quad (22)$$

IV. EXPERIMENTAL RESULTS

The overall speed sensorless control scheme is shown in Fig.6. The control scheme contains an outer speed loop and inner current loops with i_d^*, i_x^* and $i_y^* = 0$. Estimated position $\hat{\theta}$ and estimated speed $\hat{\omega}$ are obtained from algorithm mentioned above and then will be used for the control.

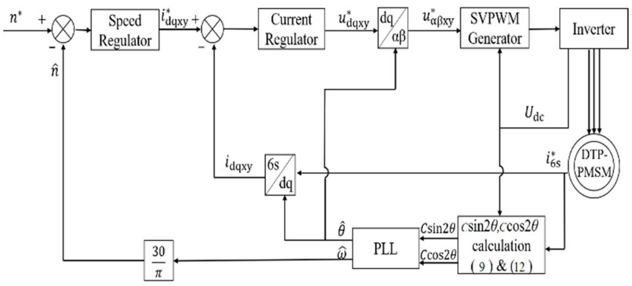

Fig.6 Block diagram of overall sensorless speed controlled DTP PMSM system (C=C_1 or C_2)

The experimental test bench contains a controller board based on TMS320F28379 DSP, a six-phase two-level inverter, a DTP PMSM coupled with an AC machine for loading and its dynamometer controller. The experimental test bench is shown in Fig.7. The dc-link voltage was set to 150 V, and the PWM frequency was set to 2.5 kHz, with a minimum pulse width 40 µs for the motor mainly due to the large current measurement noise in the test bench. An encoder (4086 *ppr*) was installed for verification of the rotor position estimation methods. The specifications and controller parameters of the DTP PMSM drive are shown in Table II. The DTP PMSM was manually wound by the authors. For the safety's sake, the following operation limitations were applied: torque 3 NM, RMS current 5 A, speed 1000 rpm, and voltage 100 V.

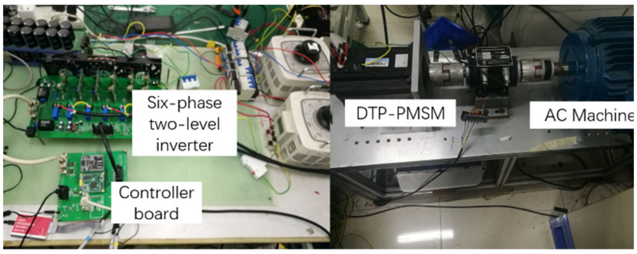

Fig.7 Experimental test bench

TABLE II
Specifications of the DTP PMSM

Machine Parameters	Values
Phase resistance	0.125Ω
d-axis inductance	1.8 mH
q-axis inductance	3.3 mH
flux linkage	0.2307 Wb
Pole pairs	5
Slot numbers	12
Stator Inner Diameter	6.6 cm
Stack length	14 cm
DC-link voltage	150 V

All the waveforms except the current in following sections were all obtained by the three inherent DACs (Digital Analog Converter) of the DSP, which indicates that up to three signals in the DSP could be observed simultaneously. The current waveform was obtained by the PT-710D current probe with a 1.5 MHz bandwidth. The current transducers used in the test rig are of LAH 25NP produced by LEM, with an accuracy of ±0.3 % and a 200 kHz bandwidth. The torque meter, JN338-A, in the test rig is a product of Beijing Xinyuhan Measurement&CT Co.LTD, with an accuracy of 0.5 %.

C. Experimental Results on Minimum Pulse Width Compensation and the Rotor Position Vector Signals

The effect of minimum pulse width compensation using the method described in Section III-A is further tested. The comparison results without and with the compensation method are shown in Fig. 8 and Fig. 9, where i_q and i_q^* refer to the actual and reference q axis currents respectively.

From Fig.8 and Fig.9, it can be proved that the compensation method in this paper is valid and necessary. i_q tracked i_q^* well with the compensation method, while i_q suffered from an offset without compensation. The compensation measures effectively ensure that the synthetic vector follows the reference vector in the case that the dwell time of first two non-zero vectors are extended.

The fluctuation range of i_q was about 1.6 A without compensation, while 0.4A with compensation in steady state.

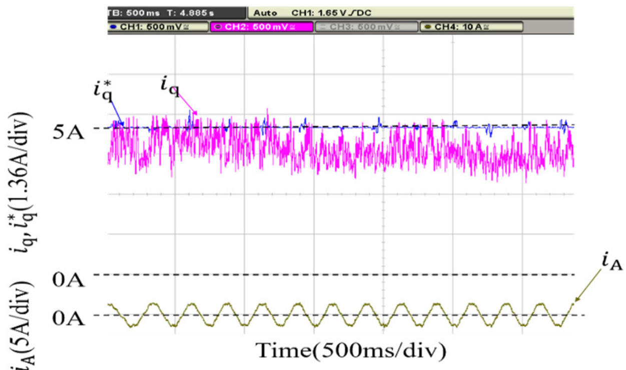

Fig. 8 i_q, i_q^* and i_A waveforms without the compensation method (4 Hz)

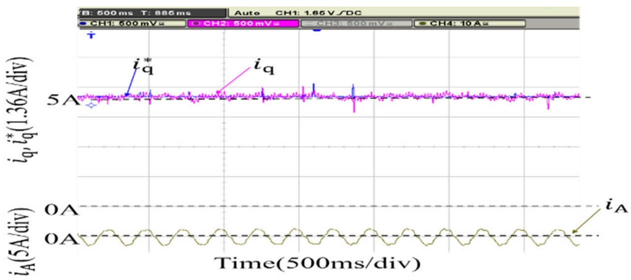

Fig.9 i_q, i_q^* and i_A waveforms with the compensation method (4 Hz)

The constructed rotor position signals with the least square method are shown in Fig.10 and Fig.11. Fig. 10 shows the rotor position vector in the α-β subspace. Fig. 11 shows the rotor position vector in the x-y subspace.

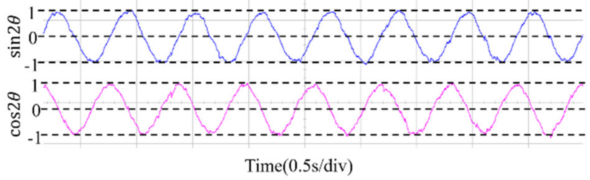

Fig. 10 sin2θ and cos2θ waveforms obtained by the oversampling method in the α-β subspace at 10 rpm (0.83 Hz)

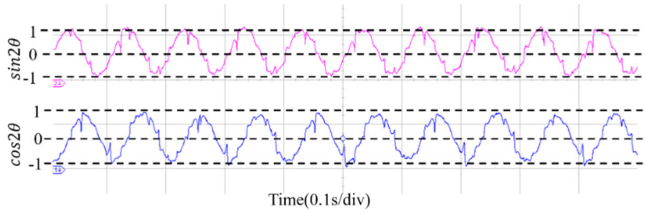

Fig. 11 sin2θ and cos2θ waveforms obtained by the oversampling method in the x-y subspace at 60 rpm (5 Hz)

The rotor position vector in the x-y subspace contains more harmonics than that in the α-β subspace. The reason will be explained in Subsection E.

D. Sensorless Experimental Results in the α-β Subspace

Closed-loop sensorless speed operation of the DTP-PMSM with the rotor position estimated in the α-β subspace has been performed, and the results are given below.

Figs. 12 and 13 illustrate the low speed operation of the motor.

Fig.12 shows the speed control at 12 r/min (1Hz) with a dynamic load from 0 Nm to 2 Nm at t≈1.75 s. The rotor angle was distorted upon the load step, but soon recovered after the load step. In Fig. 13, the motor underwent a speed step from zero to 12 rpm (1Hz) under 2 Nm load.

Fig.14 shows the speed control at 1000 r/min (83.3Hz) under no load. No obvious distortion in the rotor angle is present.

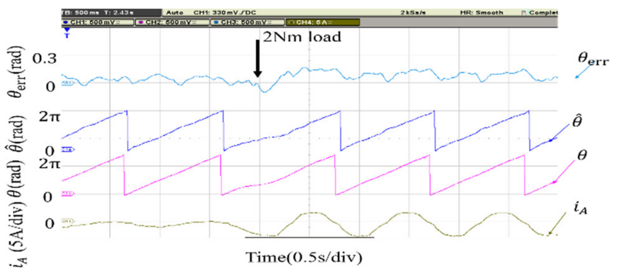

Fig. 12 Rotor position estimation at 12 r/min (1 Hz) with a load from no load to 2 Nm in the α-β subspace

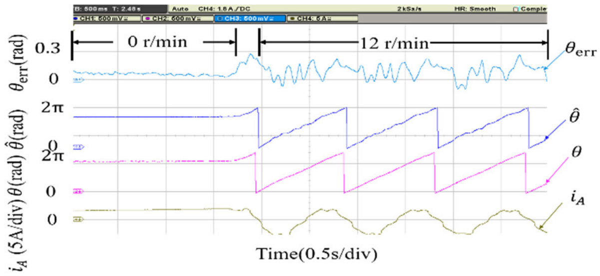

Fig. 13 Rotor position estimation from 0 r/min to12 r/min (1 Hz) with a 2 Nm load in the α-β subspace

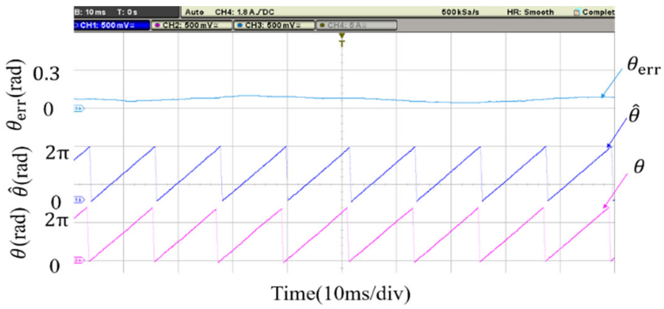

Fig. 14 Rotor position estimation at 1000r/min (83.3Hz) in the α-β subspace

From the results above, the steady state estimation error in the α-β subspace was less than 0.3 rad in both low and higher speed operation conditions. It can be concluded that the position estimation method based on the α-β subspace worked well at both low and higher speeds.

E. Sensorless Experimental Results in the x-y Subspace

During the tests, it was found out that the constructed rotor position signals contained some harmonics, which were supposed to come from the non-ideal leakage inductance. The main low order harmonics are found to be 4,5 and 7 of the fundamental frequency. These harmonics were mitigated with the synchronous filter technique with the memory algorithm disabled [33], which indicates that the rotor position estimation at very low and zero speed operation tends to be sub-satisfactory.

Fig.15 shows the speed change from 24 r/min (2Hz) to 60 r/min (5Hz) under a 2 Nm load, starting from t≈1.5 s, and settling about 0.3 s later.

Fig.16 shows the steady state sensorless speed operation at 1000 r/min (83.3Hz) under no load. Uniform distribution of both the estimated and measured rotor angles indicates stable control of the rotor speed.

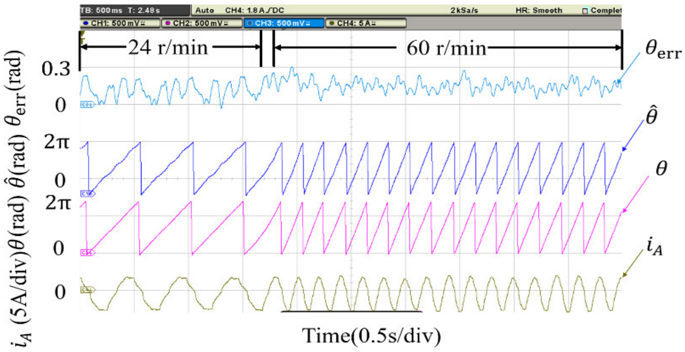

Fig. 15 Rotor position estimation from 24 r/min (2Hz) to 60 r/min (5Hz) under a 2 Nm load in the *x-y* subspace

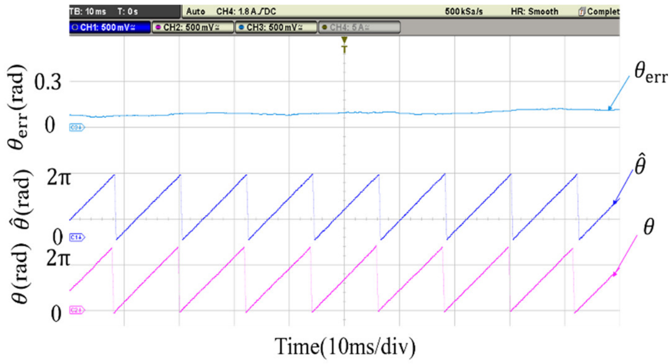

Fig. 16 Rotor position estimation at 1000 r/min (83.3Hz) under no load in the *x-y* subspace

From the results above, the estimation error in the *x-y* subspace is similar to that obtained in the *α-β* subspace. The steady estimation error in the *α-β* subspace was less than 0.3 rad in both low and higher speed operation condition. It can be concluded that the rotor position estimation method based on the *x-y* subspace also worked well from low to higher speeds.

From Figs. 14 and 16, one may notice that at 1000 rpm, the estimated rotor position gets smoother, compared with that at lower speeds. This is mainly attributed to the PLL that is capable of suppressing higher frequency noise.

THDs of the current in Figs. 12,13 and 15 under steady state and loaded conditions have been analysed, and the results are given in Tab. III.

TABLE III
THD OF THE PHASE CURRENT

Figure number	THD
Fig. 12	6% after the load step
Fig. 13	18.87% at 12 rpm
Fig. 15	8.28% at 24 rpm
	12.1% at 60 rpm

It can be seen that In Fig. 13, where the motor underwent a speed step from zero to 12 rpm, the phase current exhibits the largest THD, while in other tests, the current THDs are more or less similar. The abnormal THD in Fig. 13 is likely due to the rotor speed's transients upon the speed step. This phenomenon can also be observed in the test of Fig. 15.

V. CONCLUSIONS

Aiming at a dual three-phase PMSM, this paper reports the principles of the rotor position estimation as well as the key implementation aspects including current sampling techniques and minimum pulse width compensation method. It is demonstrated that for a DTP PMSM, the rotor position estimation is possible not only in its torque-producing (*α-β*) subspace, but also in its harmonic (*x-y*) subspace, at low and zero, as well as at higher speeds.

It is found out that in the harmonic subspace, rotor position estimation at higher speeds are possible without measuring the current derivatives of zero voltage vectors. Considering the unique feature of the dual three-phase PMSM, it becomes nature to combine these two methods together, i.e., the method in the *α-β* subspace for the low speed range and the method in the *x-y* subspace for higher speed range, to achieve a wide speed rotor position estimation. A switching algorithm between them will then be needed.

VI. DISCUSSIONS

Ideally, the two methods could both work at higher inverter switching frequencies. But at higher frequencies, for the oversampling technique, the number of samples might be limited due to the minimum A/D conversion time, and the rotor position signal quality could get reduced. This problem could be overcome by introducing faster A/D hardware, such as an FPGA. Meanwhile, for the two-point sampling technique, the samples could be interfered by the switching noises, which is much related to the hardware design of the drive system, at higher switching frequencies.

In summary, the maximum inverter switching frequency largely depends on the hardware design, the saliency ratio of the motor and the current derivative measurement hardware. For this prototyped DTP PMSM drive, best results were obtained with the PWM switching frequency at 2.5 kHz.

Finally, a comparison between the proposed method with the existing methods in terms of noise rejection, parameters uncertainties and estimation error is briefed below.

The fundamental model based (FMB) methods are free from extra noise, compared with the HF injection or the proposed methods (FPE), as no modification at all to the PWM waveforms is required, while the difference of noise emission between the HF injection and the proposed methods largely relies on such factors as practical implementation and the operational speed range. The amplitude and the frequency of the HF method, and the minimum pulse width of the FPE method, are thought to be the key factors during the practical implementation. At zero and very low speeds, it is more likely that their noise level are somewhat compatible. However, as the modification to the PWM with the FPE method tends to decrease when the operational speed increases, the resulting noise level will also become lower. On the contrary, the noise from the HF method will hardly change with speed.

Both the FPE method and the HF method are immune to the parameter uncertainties, which is not the case for the FMB methods, especially at lower speeds.

Since both the FPE method and the HF method utilize the saliency effect of the motor, the rotor position estimation error by these two methods should be very similar to each other at low and zero speeds. The error with the HF method tends to increase with speed, due to neglecting the back-emf effect and band-pass filtering. The error with the FPE method, however, will hardly change, as the back-emf effect has been considered. Meanwhile, FMB methods are supposed to perform well during medium and higher speeds, where its estimation error should be the smallest. At very low and zero speeds, the error will be enlarged so much that proper operation will become impossible.

REFERENCES

[1] R. Bojoi, M. Lazzari, F. Profumo, and A. Tenconi, “Digital field-oriented control for dual three-phase induction motor drives,” IEEE Trans. Ind. Appl., vol. 39, no. 3, pp. 752–760, May/Jun. 2003.

[2] Y. Zhao and T. A. Lipo, “Modeling and control of a multi-phase induction machine with structural unbalance,” IEEE Trans. Energy Convers, vol.11, no. 3, pp. 578–584, Sep. 1996.

[3] E. Levi, “Multiphase electric machines for variable-speed applications,” IEEE Trans. Ind. Electron., vol. 55, no. 5, pp. 1893–1909, May 2008.

[4] J. Karttunen, S. Kallio, P. Peltoniemi, P. Silventoinen, and O. Pyrhonen, "Dual three-phase permanent magnet synchronous machine supplied by two independent voltage source inverters,” Proc. Int. Symp. Power Electron., Elect. Drives, Autom. Motion, 2012, pp. 741–747.

[5] G. Rezazadeh, F. Tahami, G. -A. Capolino, Z. Nasiri-Gheidari, H. Henao and M. Sahebazamani, "Improved Design of a Six-Phase Squirrel Cage Induction Motor With Pseudo-Concentrated Windings," in IEEE Journal of Emerging and Selected Topics in Industrial Electronics, vol. 3, no. 4, pp. 1187-1194, Oct. 2022, doi: 10.1109/JESTIE.2021.3137056.

[6] Scelba G, Scarcella G, Cacciato M, et al. “Compensation of rotor positon estimation errors in sensorless dual-three phase PMSM drives through back-EMF sensing”, 2017 IEEE International Symposium on Sensorless Control for Electrical Drives (SLED). IEEE, 2017: 199-206.

[7] Liu J M, Zhu Z Q. “Rotor position estimation for dual-three-phase permanent magnet synchronous machine based on third harmonic back-EMF”, 2015 IEEE Symposium on Sensorless Control for Electrical Drives (SLED). IEEE, 2015: 1-8.

[8] Liu J, Zhu Z Q. “Rotor position estimation for single-and dual-three-phase permanent magnet synchronous machines based on third harmonic back-EMF under imbalanced situation”, Chinese Journal of Electrical Engineering, 2017, 3(1): 63-72.

[9] He Y, Hu W, Wang Y, et al. “Speed and position sensorless control for dual-three-phase PMSM drives”, 2009 Twenty-Fourth Annual IEEE Applied Power Electronics Conference and Exposition. IEEE, 2009: 945-950.

[10] Fan L, Yang T, Rashed M, et al. “Sensorless control of dual-three phase PMSM based aircraft electric starter/generator system using model reference adaptive system method”, CSAA/IET International Conference on Aircraft Utility Systems (AUS 2018). IET, 2018: 787-794.

[11] Fan L, Yang T, Rashed M, et al. “Comparative study of back EMF based sensorless control methods for dual three-phase PMSM”, 2018 IEEE International Conference on Electrical Systems for Aircraft, Railway, Ship Propulsion and Road Vehicles & International Transportation Electrification Conference (ESARS-ITEC). IEEE, 2018: 1-6.

[12] Almarhoon A, Ren Y, Zhu Z Q. “Influence of back-EMF and current harmonics on sensorless control performance of single and dual three-phase permanent magnet synchronous machines”, Compel: International journal for computation and mathematics in electrical and electronic engineering, 2016, 35(2): 744-763.

[13] Yu H, Gan C, Wang H, et al. “Speed Adaptative Sensorless Control Method of a High-speed Dual Three-phase Permanent Magnet Synchronous Motor”, 2020 23rd International Conference on Electrical Machines and Systems (ICEMS). IEEE, 2020: 155-160.

[14] S. R and B. Singh, "Sensorless Predictive Control of SPMSM-Driven Light EV Drive Using Modified Speed Adaptive Super Twisting Sliding Mode Observer With MAF-PLL," in IEEE Journal of Emerging and Selected Topics in Industrial Electronics, vol. 2, no. 1, pp. 42-52, Jan. 2021, doi: 10.1109/JESTIE.2020.3014866.

[15] Roetzer M, Vollmer U, Chen L, et al. “Anisotropy-based position estimation approach for symmetrical dual three-phase permanent magnet synchronous machines”, 2017 IEEE International Symposium on Sensorless Control for Electrical Drives (SLED). IEEE, 2017: 157-164.

[16] Barcaro M, Faggion A, Bianchi N, et al. “Predicted and experimental anisotropy of a dual three-phase interior permanent magnet motor for sensorless rotor position control”, 6th IET International Conference on Power Electronics, Machines and Drives (PEMD 2012). IET, 2012: 1-6.

[17] Barcaro M, Faggion A, Bianchi N, et al. “Sensorless rotor position detection capability of a dual three-phase fractional-slot IPM machine”, IEEE Transactions on Industry Applications, 2012, 48(6): 2068-2078.

[18] Wang S, Imai K, Doki S. “Analysis of an Application of the Extended Electromotive Force Model Based Position Sensorless Control on the Wound-Field Synchronous Motor with Dual-Three Phases in Standstill/Low Speed Region”, IECON 2018-44th Annual Conference of the IEEE Industrial Electronics Society. IEEE, 2018: 5789-5794.

[19] Bin X, Luo X, Zhu L, et al. “Sensorless Control of Dual Three-Phase PMSM with High Frequency Voltage Signal Injection”, 2019 22nd International Conference on Electrical Machines and Systems (ICEMS). IEEE, 2019.

[20] Almarhoon A H, Zhu Z Q, Xu P. “Improved rotor position estimation accuracy by rotating carrier signal injection utilizing zero-sequence carrier voltage for dual three-phase PMSM”, IEEE Transactions on Industrial Electronics, 2016, 64(6): 4454-4462.

[21] Almarhoon A H, Zhu Z Q, Xu P L. “Improved pulsating signal injection using zero-sequence carrier voltage for sensorless control of dual three-phase PMSM”, IEEE Transactions on Energy Conversion, 2017, 32(2): 436-446.

[22] Liu T, Zhu Z Q, Wu Z Y, et al. “A Simple Sensorless Position Error Correction Method for Dual Three-Phase Permanent Magnet Synchronous Machines”, IEEE Transactions on Energy Conversion, 2020.

[23] Gao Q, Asher G M, Sumner M, et al. “Position estimation of AC machines over a wide frequency range based on space vector PWM excitation”. IEEE Transactions on Industry Applications, 2007, 43(4): 1001-1011.

[24] Hua Y, Sumner M, Asher G, et al. “Improved sensorless control of a permanent magnet machine using fundamental pulse width modulation excitation”. IET Electric Power Applications, 2011, 5(4): 359-370.

[25] Bui M X, Guan D, Xiao D, et al. “A modified sensorless control scheme for interior permanent magnet synchronous motor over zero to rated speed range using current derivative measurements”. IEEE Transactions on Industrial Electronics, 2018, 66(1): 102-113.

[26] M. Ahmad, Wen Zhang and Q. Gao, "Low and zero speed position estimation of dual three-phase PMSMs based on the excitation of PWM waveforms," *2017 IEEE 3rd International Future Energy Electronics Conference and ECCE Asia (IFEEC 2017 - ECCE Asia)*, Kaohsiung, 2017, pp. 1652-1658.

[27] Hao Chen, Qiang Gao and Haoyue Zhu, “Low and zero speed sensorless control of dual three-phase permanent magnet synchronous machines using the fundamental PWM excitation”, 10th IET International Conference on Power Electronics, Machines and Drives, PEMD 2020, Nottingham, UK.

[28] Zhao Y, Lipo T A. “Space vector PWM control of dual three-phase induction machine using vector space decomposition”, IEEE Transactions on industry applications, 1995, 31(5): 1100-1109.

[29] H. S. Che, E. Levi, M. Jones, W. -P. Hew and N. A. Rahim, "Current Control Methods for an Asymmetrical Six-Phase Induction Motor Drive," IEEE Transactions on Power Electronics, vol. 29, no. 1, pp. 407-417, Jan. 2014, doi: 10.1109/TPEL.2013.2248170.

[30] Grandi G, Serra G, Tani A. “Space vector modulation of a six-phase VSI based on three-phase decomposition”, 2008 International Symposium on Power Electronics, Electrical Drives, Automation and Motion. IEEE, 2008: 674-679.

[31] Duan Y, Sumner M. “A novel current derivative measurement using recursive least square algorithms for sensorless control of permanent magnet synchronous machine”, Proceedings of The 7th International Power Electronics and Motion Control Conference. IEEE, 2012, 2: 1193-1200.

[32] Raja R, Sebastian T, Wang M. “Practical implementation of current derivative measurement for sensorless control of permanent magnet

machines", 2018 IEEE Transportation Electrification Conference and Expo (ITEC). IEEE, 2018: 1-6.

[33] Gao Q, Asher G, Sumner M. "Sensorless position and speed control of induction motors using high-frequency injection and without offline precommissioning", IEEE Transactions on Industrial Electronics, 2007, 54(5): 2474-2481.